Energy & Environmental Science

ROYAL SOCIETY OF CHEMISTRY

PAPER

View Article Online
View Journal

Cite this: DOI: 10.1039/d0ee01102a

Self-powered electrocatalytic ammonia synthesis directly from air as driven by dual triboelectric nanogenerators†

Kai Han,[ab] Jianjun Luo,[ab] Yawei Feng,[ab] Liang Xu,[abc] Wei Tang*[abc] and Zhong Lin Wang *[abd]

Received 14th March 2020,
Accepted 19th June 2020

DOI: 10.1039/d0ee01102a

rsc.li/ees

Electrocatalytic reduction at room temperature and atmospheric pressure is a promising low-power-consumption and eco-friendly pathway for replacing the traditional ammonia synthesis method, which is one of the largest chemical processes in terms of energy consumption and greenhouse gas emissions. In this work, we utilize triboelectric nanogenerators (TENGs) to construct an electrocatalytic ammonia synthesis system with air as the nitrogen source, which is self-powered, eco-friendly, low-cost, scalable and allows facile fabrication. The nitrogen fixation and electrocatalytic reduction can proceed simultaneously by introducing a high-output dual-TENG configuration. A needle-plate structure was utilized to achieve air discharge and thus obtain NO_X for further aqueous electrolyte formation. In addition, an electrochemical cell with TiO_2 as the catalyst was used to synthesize ammonia. Driven by the simulated waste gas at a flow rate of 3.5 m^3 min^{-1}, the ammonia yield per hour of the self-powered electrocatalytic system reached 2.4 μg h^{-1}.

Broader context

The high demand for ammonia, as one of the largest inorganic productions in the world, has led to huge consumption of energy and plenty of relevant environmental pollution problems, which cause great pressure on our society. It is urgent to develop energy-saving and eco-friendly methods for ammonia synthesis. By introducing a high-output dual triboelectric nanogenerator (TENG) configuration, a self-powered electrocatalytic ammonia synthesis system was constructed to achieve this. In this system, the whole synthetic process can proceed under ambient conditions. Instead of the high purity N_2 requirement in other methods, air can be directly used as a nitrogen source by simple discharging caused by one TENG. The fixation product is then utilized to form the electrolyte solution for the synchronous electrocatalytic synthesis of ammonia driven by the other TENG, involving a non-noble-metal catalyst. Furthermore, with the help of a turbocharger, it is feasible to reuse the residual kinetic energy of the exhaust gas from factories to drive the ammonia synthesis system. Compared with traditional synthetic methods, this system possesses the advantages of being self-powered, eco-friendly, low-cost, and scalable, with facile-fabrication, showing great potential for ammonia synthesis.

Introduction

As one of the largest inorganic productions in the world, ammonia has played an important role in fertilizer-making and the production of other chemicals.[1] Correspondingly, ammonia synthesis consumes huge quantities of fossil fuels. Besides, represented by the Haber–Bosch process, traditional synthetic methods require harsh conditions such as high temperature and high pressure, which increase the demand for energy and cause harm to the environment.[2] Therefore, the search for low-power-consumption and eco-friendly methods is urgent and electrochemical reduction at room temperature and atmospheric pressure, especially in aqueous electrolyte, is a promising pathway for achieving this.[3,4]

Since it is a great challenge to break the stable nitrogen–nitrogen triple bond due to its high bond energy (940.95 kJ mol^{-1}) under ambient conditions,[5] current studies focus more on electrocatalysts for the reduction of N_2 to ammonia. Recently, various materials such as noble metals (Pd, Au, *etc.*), normal

[a] *CAS Center for Excellence in Nanoscience, Beijing Institute of Nanoenergy and Nanosystems, Chinese Academy of Sciences, Beijing 100083, P. R. China. E-mail: tangwei@binn.cas.cn*
[b] *School of Nanoscience and Technology, University of Chinese Academy of Sciences, Beijing 100049, P. R. China*
[c] *Center on Nanoenergy Research, School of Physical Science and Technology, Guangxi University, Nanning 530004, P. R. China*
[d] *School of Material Science and Engineering, Georgia Institute of Technology, Atlanta, Georgia 30332-0245, USA. E-mail: zlwang@gatech.edu*

† Electronic supplementary information (ESI) available. See DOI: 10.1039/d0ee01102a

metals and metallic compounds (Cu, TiO_2, MoS_2, *etc.*) and non-metallic materials (black phosphorus, COF, *etc.*) have been utilized and show good electrocatalytic performance under a constant electric drive (Table S1, ESI†). Zhang *et al.*[6] used black phosphorus nanosheets as an efficient non-metallic catalyst, which achieved a high NH_3 yield of 31.37 μg h^{-1} $mg_{cat.}^{-1}$ at −0.7 V *vs.* the reversible hydrogen electrode (RHE). By using defect-rich MoS_2, Li *et al.*[7] also showed outstanding performance with a yield of 29.28 μg h^{-1} $mg_{cat.}^{-1}$ at −0.40 V *vs.* RHE. However, for a new catalyst, there are varied sources of potential experimental artefacts that need to be dealt with for reliable proof, such as interferences from labile nitrogen-containing compounds and even the catalyst itself in the system.[8–10] To avoid the influence of oxygen and increase the amount of nitrogen in the electrolyte, the requirement for a high purity nitrogen source is another issue.[11,12] Although some researchers have tried using air or wet air for the ammonia synthesis, additional heating is usually needed in these systems, even over 400 °C (Table S1, ESI†). Apart from electrocatalytic N_2 reduction, other nitrogen-rich compounds such as nitrates and nitrites are reduced to ammonia for wastewater treatment.[13,14] Nevertheless, because of the complex composition of wastewater, there will be a series of intractable problems, from the selective catalysis to the later extraction. Thus, it is significant to seek other ways to realize bond breaking and ammonia synthesis from the perspective of energy, catalytic reduction and process controllability.

Originating from Maxwell's displacement current, the triboelectric nanogenerator (TENG) is a developing technology in energy harvesting with huge practical value.[15–18] Based on a series of advantages such as a wide range of material sources and simple fabrication, various TENGs have been utilized to convert multiform mechanical energy into electrical energy for different applications,[18–23] including self-powered electrochemical reactions.[24–26] Besides, due to the high voltage property of TENG, it can easily build a strong electric field to realize chemical bond breaking, including nitrogen fixation.[27,28] Furthermore, since billions of tons of flue gas are exhausted into the air every year,[29] the residual gas kinetic energy can be used for self-powered synthesis before emission.

In this work, taking advantage of the high-voltage of the TENG, nitrogen fixation is simply realized by directly using air as the source, which is distinguished from electrocatalytic N_2 reduction. In addition, the self-powered characteristics of the TENG lead to non-noble-metal electrocatalytic reduction, in which no extra electrolyte addition and no power are needed. In particular, by using air discharge induced by the high voltage from the TENG, nitrogen and oxygen are ionized and fixed into NO_X. The gas flow with NO_X is washed by water and directly forms an electrolyte containing NO_3^- and NO_2^- for further reaction. Additionally, driven by the other simultaneously working TENG, electrocatalytic reduction is carried out to synthesize ammonia in an electrochemical cell. All of these can be simply achieved by the power of simulated waste gas at room temperature and atmospheric pressure.

Results and discussion

Fig. 1a shows a structure diagram of the dual-TENG device for self-powered ammonia synthesis. Two disk-structure TENGs in non-contact-sliding freestanding mode were assembled vertically with a common drive shaft. The stator was a PCB circuit board with 6 pairs of Cu electrodes in parallel connection fixed on an aluminum plate. The rotor was composed of 6 separate Kapton films on a substrate of epoxy glass cloth board (FR-4). To reduce rotational inertia for less energy consumption and

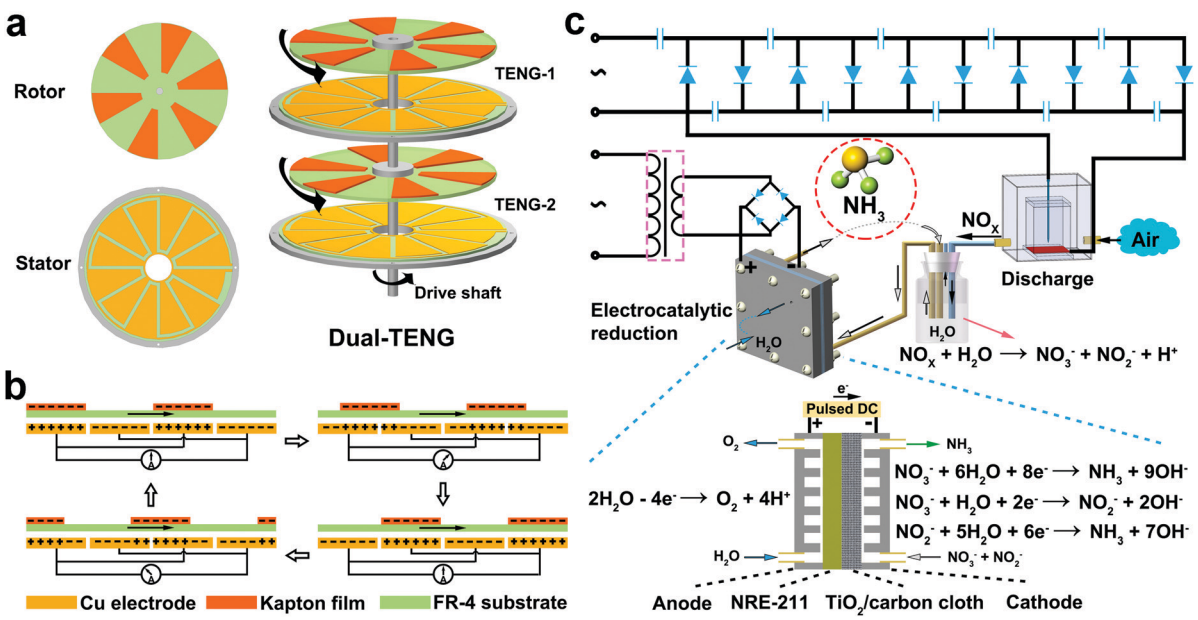

Fig. 1 Schematic diagram. (a) Construction of the dual-TENG device. (b) Working principle of the TENG. (c) Ammonia synthesis devices, main reaction processes and mechanisms.

sufficient mechanical strength, a thickness of 0.3 mm of FR-4 was selected. Before the device was assembled, the Kapton film was initially negatively charged by rubbing with the Cu film. There was a small gap between the rotor and the stator to reduce the friction resistance for high-speed rotation. The power generation principle of the non-contact-sliding free-standing mode TENG in the short-circuit state is shown in Fig. 1b. Two pairs of electrodes were drawn to help describe the mechanism. Since the Kapton film was negatively precharged, positive charges were induced in the electrode right below. In the first half cycle of electricity generation, as the rotor slides, the positive charges will flow from the first electrode to the next in the circuit until the Kapton reaches the overlapping position of the next electrode. As the sliding continues, the induced positive charges will keep flowing to the next electrode in the same way. Since the electrodes are connected in parallel, the current direction reverses in the circuit. When the first Kapton film is on the overlapping position of the first electrode in the second pair, a whole cycle of the electricity generation process is complete. The devices and corresponding main reaction processes and mechanisms are illustrated in Fig. 1c. To break the strong nitrogen–nitrogen bond, a typical discharge device with a needle-plate structure was employed. Besides, a ten-stage voltage multiplier circuit was connected to TENG-1 to achieve a higher voltage. As TENG-1 works, a strong electric field is generated and can excite and ionize nitrogen and oxygen molecules in the space between the needle and plate. The discharge process is an important step in fixing nitrogen and producing NO_X.[30,31] The air was continuously flowed through the device and then into a gas-washing bottle containing water, thus producing an electrolyte containing NO_3^- and NO_2^-. Meanwhile, with circuit management by a transformer and a rectifier, TENG-2 can be simply viewed as a pulsed DC power to drive the subsequent electrocatalytic reduction for ammonia synthesis. As for the cathode region, NO_3^- can be reduced to NH_3 directly or first to NO_2^-; the newly produced and pre-existing NO_2^- can be further reduced to NH_3. As for the anode region, oxygen is the main product of the oxidation of water.

Tested by an electrometer and a multimeter with high-voltage attenuation, the basic performance of the dual-TENG device is shown in Fig. 2. A high-speed motor with a controller was used as the simulated driving force. As shown in Fig. 2a–f, both TENG-1 and TENG-2 demonstrated high output performance with no significant difference. With the increase in the motor speed, the transferred charge and short-circuit current gradually became larger and reached about 1 μC and 0.55 mA at a speed of 5000 r min^{-1}, respectively. Meanwhile, the open-circuit voltage of both TENGs remained relatively stable in the range of 630–720 V. It is worth noting that there should be no speed dependency for the transferred charge based on the fundamental theory of sliding freestanding TENG.[17] Since the ratio of the thickness to the diameter of the FR-4 substrate was 0.15%, it was hard to keep it horizontal all the time. Thus, there was unwanted friction with Cu electrodes, especially at a low rotation speed. The positive charge generated on the FR-4 weakened the induced electric field and reduced the transferred charge. As the speed increased, the negative effect was reduced with less friction. The maximum peak power was examined as well and is shown in Fig. S1 (ESI†).

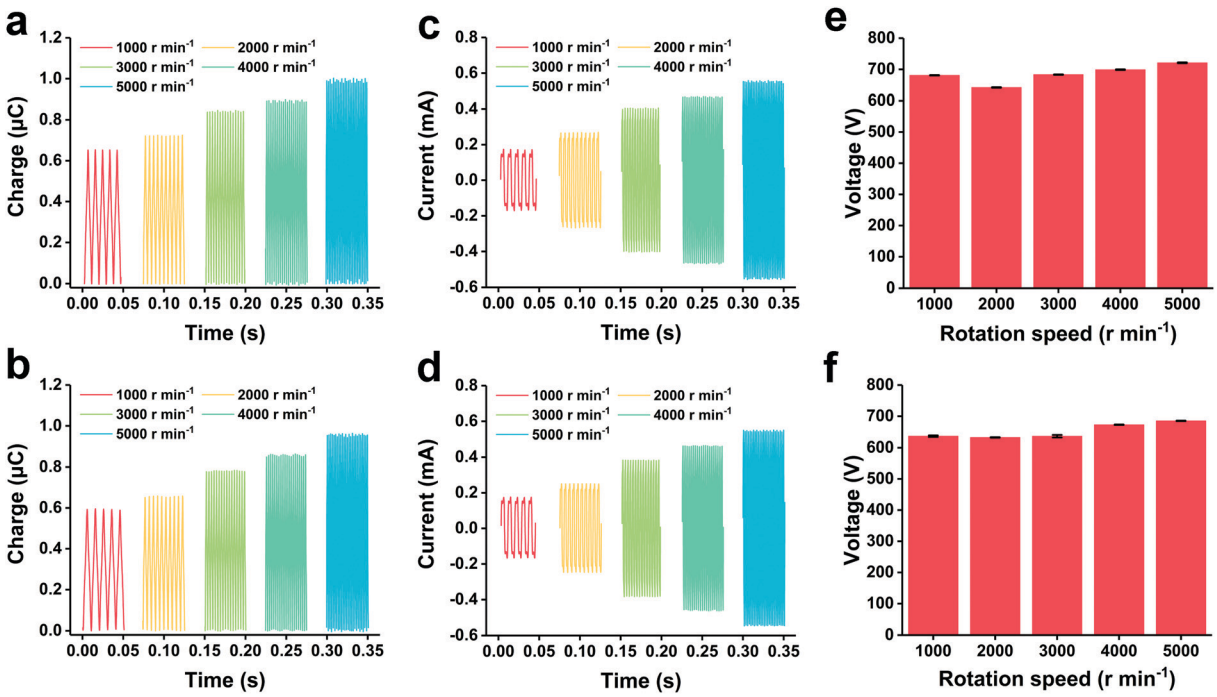

Fig. 2 (a) Transferred charge of TENG-1. (b) Transferred charge of TENG-2. (c) Short-circuit current of TENG-1. (d) Short-circuit current of TENG-2. (e) Open-circuit voltage of TENG-1. (f) Open-circuit voltage of TENG-2.

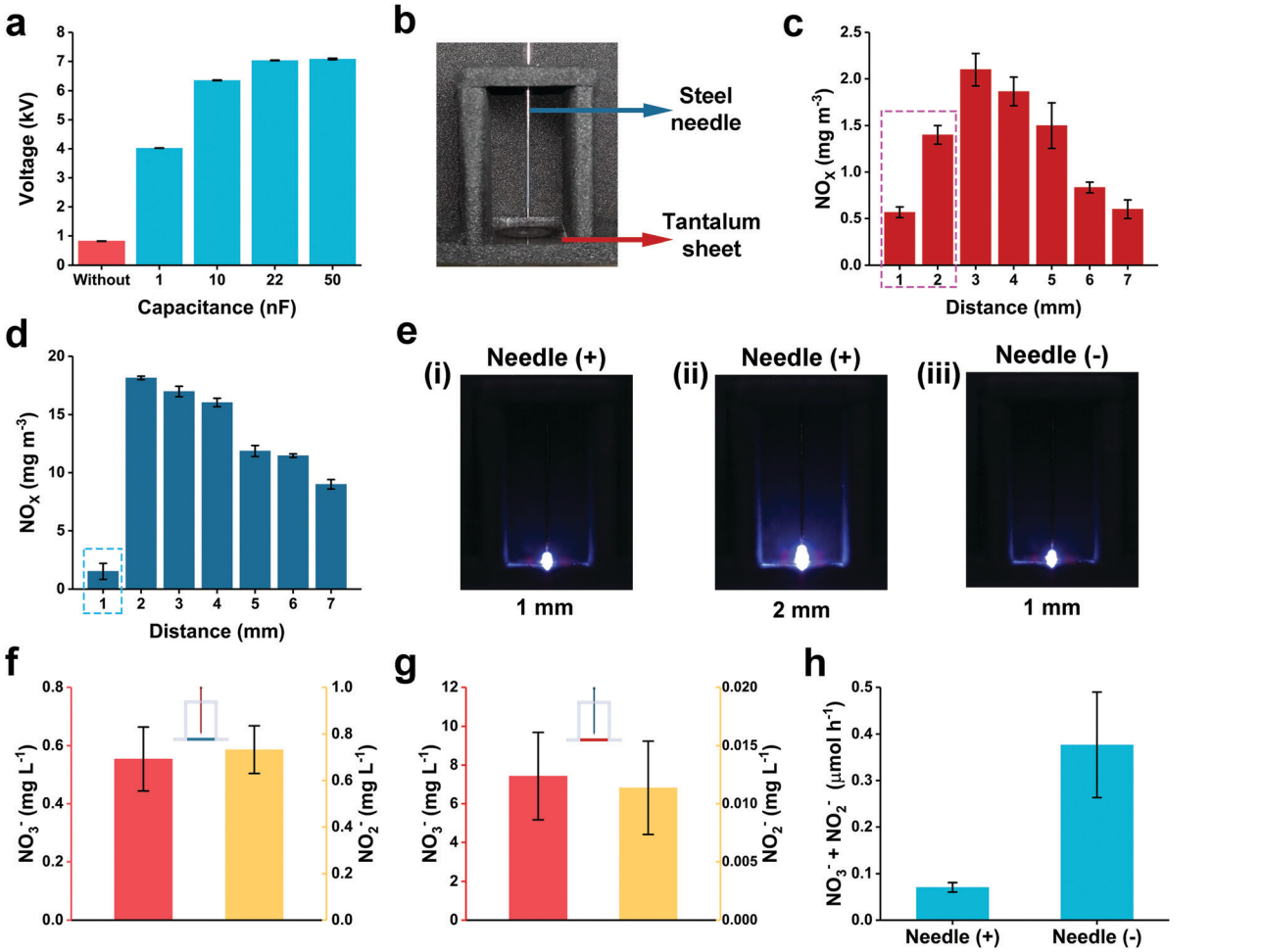

Fig. 3 (a) Voltage variation of TENG-1 using ten-stage voltage multiplier circuits with different capacitors. (b) Pictures of the air discharge device. Concentrations of NO_X using the needle (c) as the positive electrode and (d) as the negative electrode after 5 min discharge in a sealed box. (e) Typical pictures of spark discharge under different conditions. Concentrations of NO_3^- and NO_2^- using the needle (f) as the positive electrode and (g) as the negative electrode after air was discharged and passed through 20 mL of pure water for 6 h. (h) Comparison of the total water soluble ions containing nitrogen in mole yield per hour.

Although the TENGs have shown good high-voltage characteristics, a ten-stage voltage multiplier circuit containing capacitors and diodes was utilized to obtain higher voltage for better air discharge performance.[32–34] The basic working principle of this circuit is shown in Fig. S2, and more detailed information is described in the ESI.† Four kinds of high-voltage resistive capacitors with the same diodes were assembled and tested with TENG-1, respectively. As shown in Fig. 3a, a 50 nF capacity was better to help boost the voltage to an expected value of about 7 kV. It was inferred that a low capacity would not be able to store too much charge, which could lead to electric leakage and reduce the boost effect. A typical discharge structure was utilized (Fig. 3b), which contained a steel needle and a tantalum sheet as electrodes. Tantalum is a corrosion-resistant metal with non-noble properties, which is a good choice for the acid-gas environment containing NO_X. Since the multiplier circuit has the AC to DC conversion capability, the needle was used as the positive or negative electrode to explore which condition was better for NO_X production. According to Paschen's law, the distance between the tip of the needle and the bottom plate electrode was set as a control variable at atmospheric pressure. The concentration variation of NO_X is illustrated in Fig. 3c and d, which was recorded after 5 min of discharge. The distances of 3 mm and 2 mm are the respective optimal parameters for the positive and negative conditions. When the distance is larger than the optimal value, the concentration decreases, which is attributed to the weaker electric field and subsequent lower ionization in the corona discharge. As for the shorter distance, the production of NO_X is much less. It was inferred that the obvious hard light from the impulse spark discharge (Fig. 3e), which consumes a lot of energy, may be an important reason. The distance conditions of pictures (i) and (ii) correspond well to the results in the pink dotted box of Fig. 3c, and the distance conditions of picture (iii) correspond well to the results in the blue dotted box of Fig. 3d. In addition, it was observed that more NO_X products were detected when the needle was used as the negative electrode. It was inferred that strong electric fields in different directions caused different

ionizations.[35] Since an electrolyte is needed for the ammonia synthesis, the concentration in solution is more meaningful. The discharge device with a needle-plate distance of 2 mm was sealed in another smaller box with an air inlet and outlet. Airflow through the device took the generated NO_x into a gas-washing bottle with 20 mL pure water. After 6 h of discharge, the concentrations of NO_3^- and NO_2^- were determined (Fig. 3f and g) according to their standard curves (Fig. S3, ESI†). When in a positive electrode state, NO_3^- and NO_2^- were at the same concentration level of less than 1 mg L^{-1}. As for the negative electrode state, the concentration of NO_3^- was much higher and achieved 7.4 mg L^{-1}, while the concentration of NO_2^- was less than 0.02 mg L^{-1}. Since the airflow will take some water molecules away, the residual volume was also measured after each discharge (Fig. S4, ESI†). The yield per hour data are shown in Fig. 3h for comparison. Based on the results above, the condition of using the needle as a negative electrode with a needle-plate distance of 2 mm was selected.

As an effective, cheap and low-toxicity catalyst, TiO_2 is widely used in photocatalytic and electrocatalytic reactions, in which reductions of nitrate and nitrite are also involved.[36–39] Herein, a commercial nano-TiO_2 (P25) is introduced into the electrocatalytic system for ammonia synthesis. In a single cell, a carbon cloth covered by TiO_2 nanoparticles was used as the working electrode, a graphite electrode was used as the counter electrode. As a comparison, naked carbon cloth was also used for the electrochemical reduction. Fig. 4a and b show the SEM images of the carbon cloth and TiO_2/carbon cloth under different magnifications. Since the main electrolyte forms in solution were NO_3^- and NO_2^- from air discharge, KNO_3 and KNO_2 were chosen as the simulation reactants separately to verify the feasibility for ammonia synthesis. The cyclic voltammetry (CV) curve was measured in 20 mL of 100 mg L^{-1} NO_3^- or NO_2^- solution with the reference being the saturated calomel electrode (SCE) (Fig. S5, ESI†). There were distinguishable differences when TiO_2 was added. Using NO_3^- solution as the primary electrolyte, the electrocatalytic reduction results driven by DC power at −3 V for 6 h are shown in Fig. 4c and Fig. S6 (ESI†). According to the standard curve (Fig. S7, ESI†), the concentration of target product NH_3 was higher when using

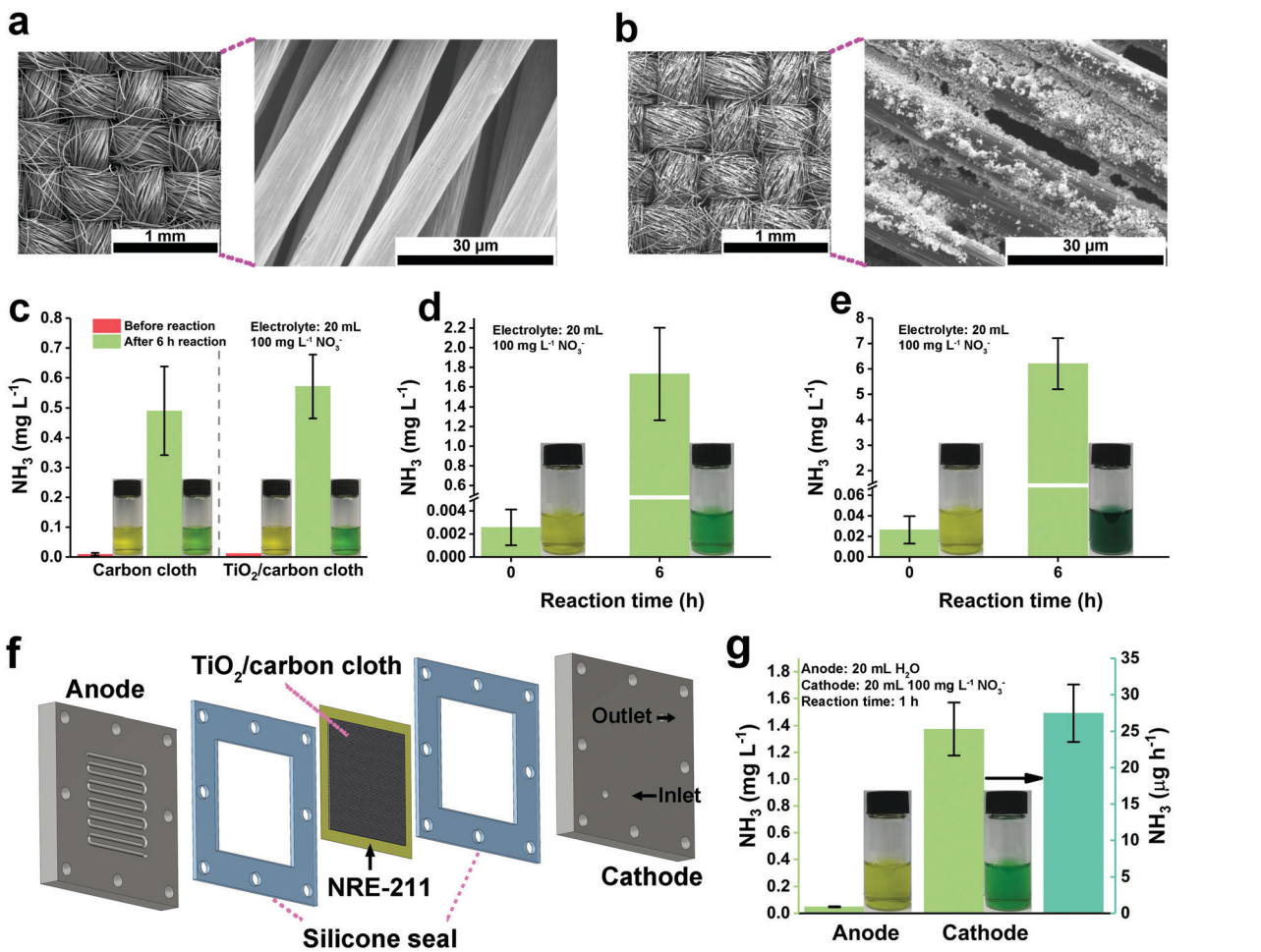

Fig. 4 (a) SEM images of carbon cloth. (b) SEM images of TiO_2/carbon cloth. Concentration variations of NH_3 using 100 mg L^{-1} NO_3^- as the electrolyte in a single cell with (c) a DC power (−3 V) drive, (d) rectified TENG-2 drive and (e) voltage step-down (350 : 12) and rectified TENG-2 drive. (f) Construction of the dual-compartment electrocatalytic cell with a fuel cell structure. (g) Concentration and mass yield per hour of NH_3 in a dual-compartment electrochemical cell with voltage step-down (350 : 4) and rectified TENG-2 drive.

TiO_2. Besides, as an intermediate product or by-product of reduction, the concentration of NO_2^- was much lower in the presence of TiO_2, which indicates better catalytic selectivity and efficiency. When directly using NO_2^- solution as the electrolyte, the results also showed a better reduction for ammonia (Fig. S8, ESI†). Another verification test using NO_3^- electrolyte at a constant current condition with −0.25 mA by an electrochemical workstation was also conducted, for which the same trend and catalytic performance were observed (Fig. S9, ESI†). The electrocatalytic system with TiO_2 was applied in the following experiments. At a rotation speed of 5000 r min^{-1}, it was clear that ammonia was synthesized, successfully driven by TENG-2 after rectification for 6 h (Fig. 4d). The concentrations of NO_3^- and NO_2^- were also determined and are shown in Fig. S10 (ESI†). To obtain more ammonia production, an electromagnetic transformer was introduced to get a higher current output for a better reduction.[25] Thus, the voltage and the current variations with different concentrations of NO_3^- and different transformer ratios were tested. In general, once the voltage can satisfy the condition to drive the reaction, a larger current is better for synthesis. As shown in Fig. S11 (ESI†), the optimal transformer ratio has a migration trend from small to large with the increase in NO_3^- concentration. A transformer ratio of 350 : 12 was selected to verify its effect. Fig. 4e shows that more ammonia was synthesized with the help of a transformer. A simple comparison of ammonia yield by different powers is shown in Fig. S12 (ESI†). With the drive of the TENG, a comparable yield to DC power can be obtained. Besides, the yield was 20.8 μg h^{-1} with the transformer, which was about 3.5 times that without. A comparison of the Faraday efficiencies is shown in Fig. S13 (ESI†). More information about the calculation is illustrated in the ESI.† The efficiency by TENG-2 was 13.9%, which is about half the value by DC power. However, it was still comparable, showing good application potential.

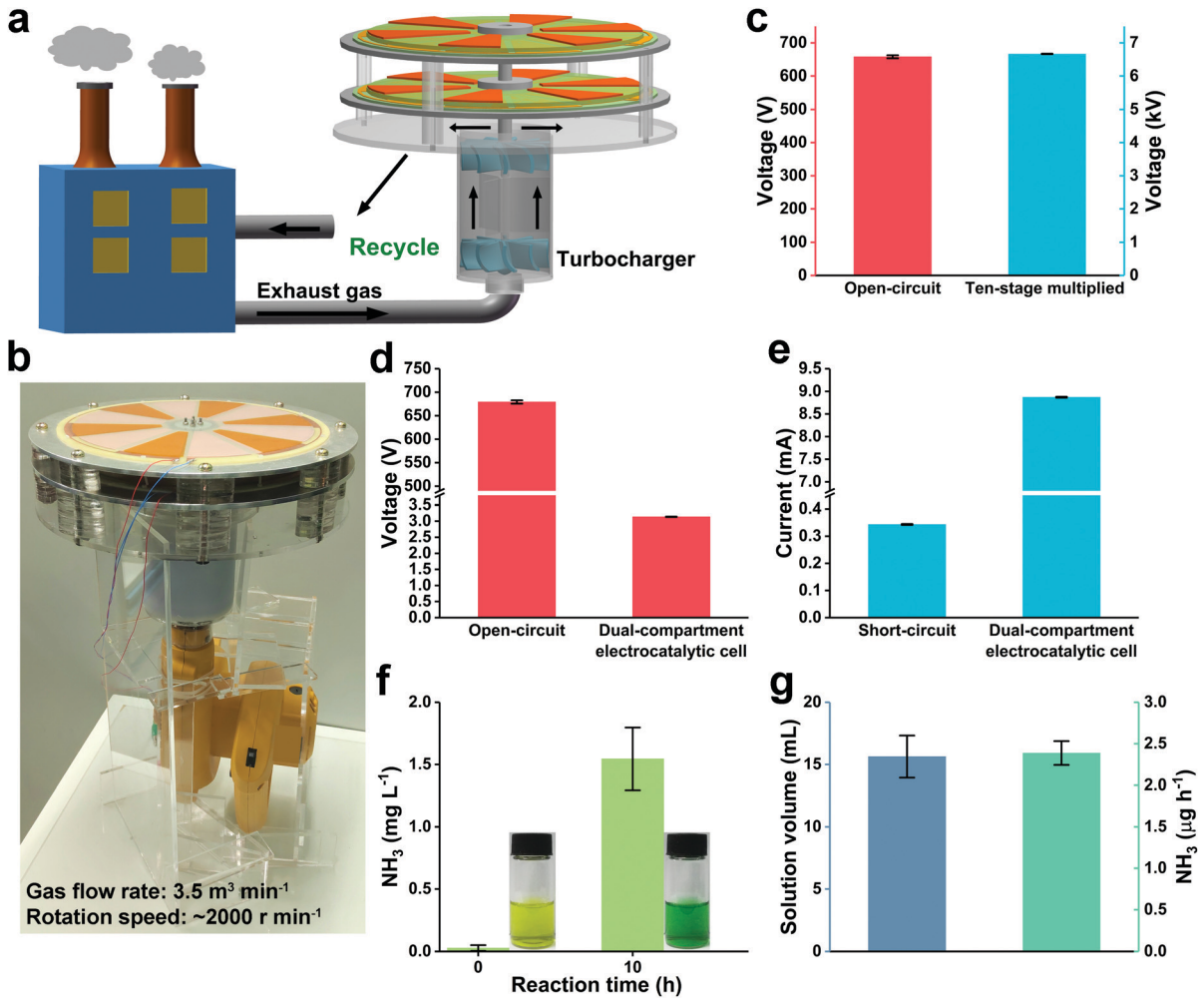

Fig. 5 (a) Schematic diagram of the self-powered dual-TENG device. (b) Picture of the self-powered dual-TENG device with a blower as the simulated exhaust gas source. (c) Open-circuit voltage and ten-stage multiplied voltage of TENG-1. (d) Open-circuit voltage of TENG-2 and voltage of the dual-compartment electrocatalytic cell with voltage step-down (350 : 5) and rectified TENG-2 drive. (e) Short-circuit current of TENG-2 and current of the dual-compartment electrocatalytic cell with voltage step-down (350 : 5) and rectified TENG-2 drive. (f) Concentration of NH_3 in the cathode compartment by self-powered synthesis for 10 h. (g) Residual solution volume in the cathode compartment and production per hour of NH_3 by self-powered synthesis for 10 h.

Here, it is significant to note that there was severe anodic corrosion with the current being up to the milliampere level (Fig. S14a, ESI†) when using a transformer. Such corrosion will cause electrolyte pollution and strong interference in the detection and further purification. After dilution, there was much less influence on the determination of NO_2^- and NH_3. However, the strong interference of absorption in the ultraviolet region still existed (Fig. S14b, ESI†). Therefore, a dual-compartment electrochemical cell with a fuel cell structure was introduced (Fig. 4f). The cell was assembled using a graphite bipolar plate, silicone seal, Nafion membrane (NRE-211) and TiO_2/carbon cloth. Pictures of the main components are shown in Fig. S15 (ESI†). The dual-compartment electrocatalytic cell is driven by the rectified TENG-2 at a rotation speed of 5000 r min^{-1}. Pure water (20 mL) and 20 mL of 100 mg L^{-1} NO_3^- solution were recycled in the anode region and cathode region, separately, for 1 h reaction by two peristaltic pumps both at a rate of 1 mL min^{-1}. Before the sustained reaction, the selection process for a suitable transformer was conducted as well (Fig. S16, ESI†) and a ratio of 350 : 4 was used. The determination results of the anode and cathode compartments after 1 h of reaction are shown in Fig. 4g. The ammonia yield per hour in the cathode area was 27.5 μg h^{-1}, which is a little higher than the reaction in a single cell. Besides, a continuous reaction for 6 h with determination every hour was tested and the result is clearly shown in Fig. S17 (ESI†).

Taking advantage of TENG, it is feasible to reuse the residual kinetic energy of billions of tons of exhaust gas from factories to supply mechanical energy, and meanwhile carry out *in situ* ammonia synthesis for factories, which is energy-saving and eco-friendly. As shown in Fig. 5a, with the help of a turbocharger, the gas flow will rotate the turbofan and shaft to make the TENG produce electric energy and be recollected for emission. Based on the above, a dual-compartment electrochemical cell with TiO_2 as the catalyst and a previously mentioned discharge device were utilized to construct a self-powered system with TENGs. The gas-washing bottle was directly connected to the cathode compartment to supply the electrolyte. To avoid the determination interference from ammonia in the air, two gas filters both with 30 mL of 0.05 M H_2SO_4 were set ahead of the discharge device. A blower was used as the simulated exhaust gas source and combined with the dual-TENG and a commercial turbocharger to drive the system for ammonia synthesis (Fig. 5b). The whole system was set at a work condition of a gas flow rate of 3.5 m^3 min^{-1}. The basic performance of the dual-TENG and other relevant information of the system at the initial stage of the reaction were tested. After calculation, the rotation speed was about 2000 r min^{-1}. Also, the best transformer ratio was chosen as 350 : 5 (Fig. S18, ESI†). Fig. 5c shows the open-circuit voltage and a ten-stage multiplied voltage of TENG-1. The open-circuit voltage and short-circuit current of TENG-2 are illustrated in Fig. 5d and e. After voltage step-down and rectification, TENG-2 outputs voltage and current for the dual-compartment electrocatalytic cell around 3.1 V and 8.9 mA, respectively. After 10 h of reaction, NH_3 was successfully synthesized by the self-powered system. The determination results are shown in Fig. 5f. By measuring the solution volume involved in the cathode reaction, the self-powered ammonia yield per hour achieved 2.4 μg h^{-1} (Fig. 5g). The concentrations of NO_3^- and NO_2^- were also determined, which are shown in Fig. S19 (ESI†).

Conclusions

In conclusion, a self-powered electrocatalytic system driven by a high-output dual-TENG device was designed to synthesize ammonia, which has special advantages in terms of reactants and electrolyte as compared to the electrocatalytic N_2 reduction. Through air discharge caused by a TENG device, nitrogen was fixed into NO_X directly, using air as the source for further electrolyte formation. Meanwhile, driven by the other TENG, the electrocatalytic reduction using TiO_2 as the catalyst was carried out to synthesize ammonia in a dual-compartment electrocatalytic cell. Under the simulated waste gas at a flow rate of 3.5 m^3 min^{-1}, the ammonia yield per hour of the self-powered electrocatalytic system was 2.4 μg h^{-1} under ambient conditions. Compared with traditional synthetic methods, the system possesses the advantages of being self-powered, eco-friendly, low-cost, and scalable, with facile-fabrication, showing great potential for ammonia synthesis.

Experimental section

Fabrication of the dual-TENG

The stator was a custom-made PCB circuit with 6 pairs of Cu electrodes and fixed on an aluminum plate. A circular region with a diameter of 40 mm was cut in the center of the PCB board for the space of the drive shaft. The distance between each electrode was 5 mm. A custom-made FR-4 board was used as the substrate disc for the rotor. The diameter of the disc was 200 mm, and the thickness was 0.3 mm. The reserved hole on it was used to connect with the shaft. For the electrode, the Kapton film (60 μm) was cut into a fan shape with an area of about 22 cm^2 and stuck on the disc with space. Then, two pairs of stators and rotors were assembled in the vertical direction with the help of PMMA baseboards to tune the height.

Measurements of the basic performance of the dual-TENG

Charge and current data at different rotation speeds were measured by an electrometer (6514, Keithley Ltd) with a LabVIEW program. Since the high voltage of the TENG exceeds the range of the electrometer, a multimeter with high-voltage attenuation (HVP-40, PINTEK Ltd) was utilized. The following experiments were conducted under the condition of 5000 r min^{-1}, including air discharge and electrocatalytic reduction sections.

Fabrication of the discharge device and relevant measurements

The discharge device was simply fabricated using a common steel needle and a tantalum sheet (2 cm × 2 cm × 0.1 mm) with a PMMA frame. To reduce the effect of reflection on the pictures, a layer of black sponge was covered on the surface of the PMMA. The spark discharge pictures were taken by a high-speed camera to show a clear phenomenon.

The discharge device and a NO_X detector (BH-90, Bosean Ltd) were placed in a sealed PMMA box. The volume of the box was about 1 L without the detector counted in. The box can be reopened to tune the distance between the needle and the bottom electrode. Besides, there were reserved inlets and outlets to help exhaust the residual gas in the box during the repeated testing by a mini vacuum pump. The device was connected to a ten-stage multiplied circuit using capacitors of 50 nF and TENG-1. Each air discharge time was 5 min, then the NO_X concentration value was recorded.

To have a better collection of discharging gas, the device was placed in a small PMMA box (4 cm × 4 cm × 4 cm) that was connected to a gas-washing bottle (25 mL) with 20 mL of pure water. The distance between the needle and the bottom electrode was set at 2 mm. A mini air pump was used to help the supply gas source. After 6 h, the air discharge, volume of the solution and concentration of NO_3^- and NO_2^- were measured in turn. The needle was used as the positive and negative electrodes, respectively.

Preparation of TiO_2/carbon cloth

The commercial carbon cloth (WOS1009, Cetech Co. Ltd) was cut into different sizes (1 cm × 1 cm and 2.5 cm × 2.5 cm). Typically, 10 mg commercial nano TiO_2 (P25) catalyst and 50 μL of Nafion solution (5 wt%) were dispersed in 1 mL of absolute ethyl alcohol by sonicating for 1 h to form a homogeneous ink. Then, a certain volume of the ink was loaded onto a piece of carbon cloth electrode (1 mg cm^{-2}) and dried under ambient conditions.

Electrocatalytic reduction in a single cell

A single electrochemical cell with 60 mL volume was used in electrocatalytic verification experiments. The anode was graphite electrode (1 cm × 1 cm × 3 mm), the cathode was naked carbon cloth or TiO_2/carbon cloth with the same size. The cyclic voltammetry curve was measured in 20 mL of 100 mg L^{-1} NO_3^- or NO_2^- solution with the reference electrode being the saturated calomel electrode, using an electrochemical workstation (CHI 660E, CHEN HUA Ltd) at a scan rate of 0.05 V s^{-1}. 20 mL of 100 mg L^{-1} NO_3^- and 10 mg L^{-1} NO_2^- solutions were used as electrolytes for the simulated electrocatalytic reactions. Driven by a DC power at −3 V for 6 h, the concentrations of NO_3^-, NO_2^- and the target production of NH_3 were determined, respectively. Since the concentration may exceed the range of the standard curve, the solution may be diluted to make the determination according to the specific circumstance. When using TENG-2 as the power, a rectifier and a series of custom-made transformers were used before driving the catalytic reaction. Besides, a normal multimeter was utilized for quick tests of the voltage and current of the electrocatalytic system.

Fabrication of the dual-compartment cell and relevant electrocatalytic reduction

A piece of TiO_2/carbon cloth (2.5 cm × 2.5 cm) was combined with a piece of pre-activated Nafion membrane (NRE-211, 3 cm × 3 cm) by a hot press process at 140 °C for 0.5 h. The combination was assembled with two pieces of silicone and custom-made graphite bipolar plates (4 cm × 4 cm) with grooves to fabricate the dual-compartment cell. Next, 20 mL of pure water and 20 mL of 100 mg L^{-1} NO_3^- solution were recycled in the anode and cathode compartment with the help of two peristaltic pumps, both at a rate of 1 mL min^{-1}, and then both were determined after 1 h reaction driven by TENG-2.

Self-powered ammonia synthesis

A blower (STPT600-A9, STANLEY Ltd) was used as the simulated gas source. The dual-TENG was transferred from the DC rotor platform and connected to the blower by a simple turbocharger with two turbofans. The discharge device and the dual-compartment cell were assembled with TENGs to synthesize ammonia. At a flow rate of 3.5 m^3 min^{-1}, the solutions in the anode and cathode region were separately determined after 10 h reaction.

Conflicts of interest

There are no conflicts to declare.

Acknowledgements

The research was supported by the National Key R & D Project from the Minister of Science and Technology (2016YFA0202704), Youth Innovation Promotion Association, CAS, Beijing Municipal Science & Technology Commission (Z171100000317001, Z171100002017017, Y3993113DF), National Natural Science Foundation of China (Grant No. 51605033, 51432005, 5151101243, 51561145021), and China Postdoctoral Science Foundation (Grant No. BX20190324). In addition, thanks a lot for the help from Dr Jian Chen, Yu Bai and Qingsong Lai.

References

1 S. Giddey, S. P. S. Badwal and A. Kulkarni, *Int. J. Hydrogen Energy*, 2013, **38**, 14576–14594.
2 S. L. Foster, S. I. Perez Bakovic, R. D. Duda, S. Maheshwari, R. D. Milton, S. D. Minteer, M. J. Janik, J. N. Renner and L. F. Greenlee, *Nat. Catal.*, 2018, **1**, 490–500.
3 X. Cui, C. Tang and Q. Zhang, *Adv. Energy Mater.*, 2018, **8**, 1800369.
4 N. Cao and G. Zheng, *Nano Res.*, 2018, **11**, 2992–3008.
5 M.-M. Shi, D. Bao, B.-R. Wulan, Y.-H. Li, Y.-F. Zhang, J.-M. Yan and Q. Jiang, *Adv. Mater.*, 2017, **29**, 1606550.
6 L. Zhang, L.-X. Ding, G.-F. Chen, X. Yang and H. Wang, *Angew. Chem., Int. Ed.*, 2019, **58**, 2612–2616.
7 X. Li, T. Li, Y. Ma, Q. Wei, W. Qiu, H. Guo, X. Shi, P. Zhang, A. M. Asiri, L. Chen, B. Tang and X. Sun, *Adv. Energy Mater.*, 2018, **8**, 1801357.
8 S. Z. Andersen, V. Čolić, S. Yang, J. A. Schwalbe, A. C. Nielander, J. M. McEnaney, K. Enemark-Rasmussen, J. G. Baker, A. R. Singh, B. A. Rohr, M. J. Statt, S. J. Blair, S. Mezzavilla, J. Kibsgaard, P. C. K. Vesborg, M. Cargnello,

S. F. Bent, T. F. Jaramillo, I. E. L. Stephens, J. K. Nørskov and I. Chorkendorff, *Nature*, 2019, **570**, 504–508.
9 B. H. R. Suryanto, H.-L. Du, D. Wang, J. Chen, A. N. Simonov and D. R. MacFarlane, *Nat. Catal.*, 2019, **2**, 290–296.
10 C. Tang and S.-Z. Qiao, *Chem. Soc. Rev.*, 2019, **48**, 3166–3180.
11 F. Zhou, L. M. Azofra, M. Ali, M. Kar, A. N. Simonov, C. McDonnell-Worth, C. Sun, X. Zhang and D. R. MacFarlane, *Energy Environ. Sci.*, 2017, **10**, 2516.
12 Z. Sun, R. Huo, C. Choi, S. Hong, T.-S. Wu, J. Qiu, C. Yan, Z. Han, Y. Liu, Y.-L. Soo and Y. Jung, *Nano Energy*, 2019, **62**, 869–875.
13 Y. Wang, A. Xu, Z. Wang, L. Huang, J. Li, F. Li, J. Wicks, M. Luo, D.-H. Nam, C.-S. Tan, Y. Ding, J. Wu, Y. Lum, C.-T. Dinh, D. Sinton, G. Zheng and E. H. Sargent, *J. Am. Chem. Soc.*, 2020, **142**, 5702–5708.
14 Y. Wang, W. Zhou, R. Jia, Y. Yu and B. Zhang, *Angew. Chem., Int. Ed.*, 2020, **59**, 5350–5354.
15 F.-R. Fan, Z.-Q. Tian and Z. L. Wang, *Nano Energy*, 2012, **1**, 328–334.
16 Z. L. Wang, *Mater. Today*, 2017, **20**, 74–82.
17 S. Niu and Z. L. Wang, *Nano Energy*, 2015, **14**, 161–192.
18 C. Wu, A. C. Wang, W. Ding, H. Guo and Z. L. Wang, *Adv. Energy Mater.*, 2019, **9**, 1802906.
19 W. Tang, C. Zhang, C. B. Han and Z. L. Wang, *Adv. Funct. Mater.*, 2014, **24**, 6684–6690.
20 G. Zhu, P. Bai, J. Chen, Q. Jing and Z. L. Wang, *Nano Energy*, 2015, **14**, 126–138.
21 W. Tang, T. Jiang, F. R. Fan, A. F. Yu, C. Zhang, X. Cao and Z. L. Wang, *Adv. Funct. Mater.*, 2015, **25**, 3718–3725.
22 Z. L. Wang, T. Jiang and L. Xu, *Nano Energy*, 2017, **39**, 9–23.
23 X.-S. Zhang, M. Han, B. Kim, J.-F. Bao, J. Brugger and H. Zhang, *Nano Energy*, 2018, **47**, 410–426.
24 H. R. Zhu, W. Tang, C. Z. Gao, Y. Han, T. Li, X. Cao and Z. L. Wang, *Nano Energy*, 2015, **14**, 193–200.
25 Y. Feng, K. Han, T. Jiang, Z. Bian, X. Liang, X. Cao, H. Li and Z. L. Wang, *Nano Res.*, 2019, **12**, 2729–2735.
26 K. Han, J. Luo, Y. Feng, Q. Lai, Y. Bai, W. Tang and Z. L. Wang, *ACS Nano*, 2020, **14**, 2751–2759.
27 K. Zhao, G. Gu, Y. Zhang, B. Zhang, F. Yang, L. Zhao, M. Zheng, G. Cheng and Z. Du, *Nano Energy*, 2018, **53**, 898–905.
28 M.-C. Wong, W. Xu and J. Hao, *Adv. Funct. Mater.*, 2019, **29**, 1904090.
29 S. Bilgen, *Renewable Sustainable Energy Rev.*, 2014, **38**, 890–902.
30 R. Bálek and S. Pekárek, *Plasma Sources Sci. Technol.*, 2018, **27**, 075019.
31 N. Rehbein and V. Cooray, *J. Electrost.*, 2001, **51–52**, 333–339.
32 J. Cheng, W. Ding, Y. Zi, Y. Lu, L. Ji, F. Liu, C. Wu and Z. L. Wang, *Nat. Commun.*, 2018, **9**, 3733.
33 W. Liu, Z. Wang, G. Wang, G. Liu, J. Chen, X. Pu, Y. Xi, X. Wang, H. Guo, C. Hu and Z. L. Wang, *Nat. Commun.*, 2019, **10**, 1426.
34 Z. Wang, W. Liu, J. Hu, W. He, H. Yang, C. Ling, Y. Xi, X. Wang, A. Liu and C. Hu, *Nano Energy*, 2020, **69**, 104452.
35 Y. P. Raizer, *Gas Discharge Physics*, Springer, Berlin, 1991, pp. 324–375.
36 A. Pandikumar, S. Manonmani and R. Ramaraj, *Catal. Sci. Technol.*, 2012, **2**, 345–353.
37 D. E. Kim and D. Pak, *Chemosphere*, 2019, **228**, 611–618.
38 J. Gao, B. Jiang, C. Ni, Y. Qi, Y. Zhang, N. Oturan and M. A. Oturan, *Appl. Catal., B*, 2019, **254**, 391–402.
39 D. Saravanakumar, J. Song, S. Lee, N. Hur and W. Shin, *ChemSusChem*, 2017, **10**, 3999–4003.